DOI: XXXXXXXXXXXXXXXXXXXX - ISSN: XXXX-XXXX - Vol 1(1), 2020, pp: XX:XX

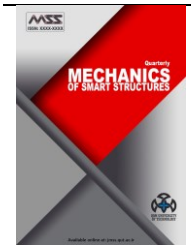

MECHANICS
OF SMART STRUCTURES
Available Online at: http://jmss.qut.ac.ir/

QOM UNIVERSITY OF TECHNOLOGY

Free damped vibration analysis of sandwich plates with MR core and GPL-reinforced face sheets

ARTICLE INFO

Article Type
Original Research

Authors
Ahmad Karbasizadeh[1]
Ali Ghorbanpour Arani[1,2,]
Shahryar Niknejad[1]

[1] Department of Solid Mechanics, Faculty of Mechanical Engineering,
[2] Institute of Nanoscience & Nanotechnology

**** Correspondence***
Address: , University of Kashan, Kashan, Iran, postal code: : 87317-53153, aghorban@kashanu.ac.ir

Article History
Received: June 21,2021
Accepted: March 12, 2022
ePublished: April 12, 2022

ABSTRACT

In this paper, an exact solution is presented for free vibration analysis of sandwich plates with magneto-rheological (MR) core and polymer-based face sheets reinforced with graphene nanoplatelets (GPLs) resting on a visco-Pasternak foundation. The set of the governing equations of motion and boundary conditions are derived using Hamilton's principle and so, are solved analytically utilizing Navier's method. The effects of various parameters on the natural frequencies and corresponding loss factor are investigated including magnetic field intensity, the aspect ratio of the sandwich plate, the thickness of the MR core and GPL-reinforced face sheets, mass fraction, aspect ratio, thickness, and distribution pattern of the GPLs, and Winkler, Pasternak, and damping coefficients of the foundation. Finally, it is shown that by increasing the magnetic field intensity from zero to a special value the natural frequencies increase and more increase in the magnetic field intensity has no remarkable effect on the natural frequencies.

Keywords: Vibration; Magneto-rheological materials; Graphene nanoplatelets; visco-Pasternak foundation.

1 Introduction

Magnetorheological materials are smart kinds of materials with controllable rheology and can be found in two forms: magnetorheological fluids (MRF) and magnetorheological elastomers (MRE). The MRs contain suspended micro-sized particles which are sensitive to applied external magnetic fields. When an MR material is subjected to a magnetic field, the arrangement of the particles changes in a uniform way which changes the mechanical properties of the materials and the mechanical characteristics can be restored when the external magnetic field is removed. There is a considerable number of papers regarding vibration analysis of the beams and plates with MR core.

Lara-Prieto et al. [1] provided an experimental study on the free vibration characteristics of cantilever sandwich beams with MR core. They confirmed the tunability of the damping and stiffness characteristics of the beams with the MR core. Nayak et al. [2] studied the dynamic buckling analysis of three-layered sandwich beams with partially MRE core and conductive skins. They concluded that as the percentage of iron particles and magnetic field increase, the stability of the structure improves. In a similar work, they focused on the dynamic stability buckling analysis of rotating three-layered sandwich beams with MRE core and conductive skins and examined the influences of the rotational speed and magnetic field on the stability regions [3]. They confirmed that applying a magnetic field to the MRE core improves the stability of the rotating sandwich beams. Using the finite element method (FEM), Rajamohan et al. [4] provided a numerical solution for the free vibrational behavior of sandwich beams with MRF core. They concluded that an increase in the applied magnetic field increases the natural frequencies and loss factors. The free vibrational characteristics of doubly tapered sandwich beams with MRE core were investigated by Navazi et al. [5]. It was shown by them that there is an optimum value of the magnetic field which maximizes the loss factor of the beam. Rokn-Abadi et al. [6] studied the influences of magnetoelastic loads on the free vibrational characteristics of the MR-based sandwich beams. They concluded that the influences of the magnetoelastic loads are more obvious with the higher beam length. Omidi Soroor et al. [7] focused on the free vibrational behavior of sandwich beams consisting of a homogenous isotropic base layer, an axially functionally graded constraining layer, and an MRF core. It was shown by them that by increasing the thickness of the MR core the natural frequencies decrease and the loss factors experience an initial steep reduction, followed by a moderate increase. Experimental and numerical results were provided by Aguib et al. [8] for the vibration analysis of sandwich plates with an MRE core. They found that an increase in the magnetic field intensity reduces the resonance amplitude. Payganeh et al. [9] focused on the free vibrational characteristics of multi-layered sandwich plates with a flexible core and MRF layers embedded between composite sheets. It was revealed by them that in order to increase the natural frequencies, it is more helpful to use thinner MRF layers. Yeh [10] studied the free vibrational behavior of orthotropic rectangular sandwich plates with MRE core and isotropic homogenous face sheets. It was shown by him that an increase in the magnetic field intensity increases the natural frequencies. The effects of MRF core on the aeroelastic stability regions of sandwich plates with MRF core were examined by Eshaghi [11]. He concluded that the critical speed of the plate

increases by increasing the magnetic field intensity.

In the current paper, the natural frequencies and corresponding loss factors are calculated analytically for the sandwich plates with MR core and GPL-reinforced face sheets resting on a visco-Pasternak foundation. The influences of various parameters on the free vibrational characteristics are examined including magnetic field intensity, the aspect ratio of the plate, the thickness of the MR core and GPL-reinforced face sheets, mass fraction, aspect ratio, thickness, and distribution pattern of the GPLs, and also Winkler, Pasternak, and damping coefficients of the foundation.

2. Mathematical modeling

As shown in Fig. 1, a sandwich three-layered rectangular plate of length b, width a resting on a visco-Pasternak foundation is considered. The face sheets are polymer-based composites reinforced with GPLs and the core is made of an MR elastomer. The thickness of the bottom, core, and top layers are shown by h_1, h_2, h_3, respectively.

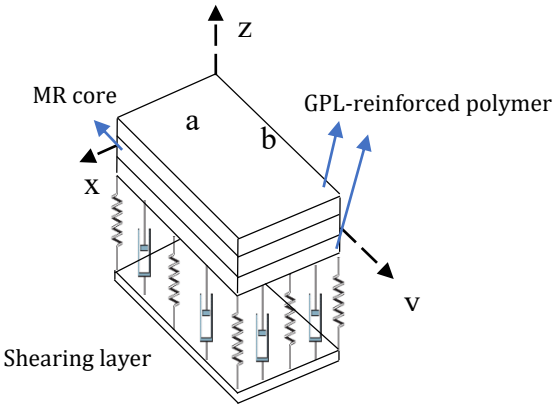

Fig. 1. Shematic of the problem

2.1 Material properties

The density (ρ) and Poisson ratio (ν) of the GPL-reinforced bottom (k=1) and top (k=3) face sheets can be calculated using the rule of mixture as [12, 13]

$$\begin{aligned}\rho^{(k)} &= \rho_{GPL}V_{GPL}^{(k)} + \rho_m V_m^{(k)} \\ \upsilon^{(k)} &= \nu_{GPL}V_{GPL}^{(k)} + \nu_m V_m^{(k)}\end{aligned} \tag{1}$$

where the subscripts m and GPL represents the matrix (polymer) and GPL reinforcements, respectively. In Eq. (1), V stands for the volume fraction which can be stated for the polymer-based matrix as

$$V_m^{(k)} = 1 - V_{GPL}^{(k)}, \tag{2}$$

and can be stated for the GPLs in terms of the mass fraction of the GPLs (g_{GPL}) as follows [12, 13]:

$$V_{GPL}^{(k)} = \frac{g_{GPL}^{(k)}}{g_{GPL}^{(k)} + \frac{\rho_{GPL}}{\rho_m}\left(1 - g_{GPL}^{(k)}\right)}, \tag{3}$$

As depicted in Fig. 2, five distribution patterns are studied in this paper. The mass fraction of the GPLs at the bottom ($-0.5h_1 \le z_1 \le 0.5h_1$) and top ($-0.5h_3 \le z_3 \le 0.5h_3$) face sheets can be stated as [14]

$$\begin{aligned}&\text{UD:} && g_{GPL}(z_k) = g_{GPL}^{*}, \\ &\text{FG-A:} && g_{GPL}(z_k) = \left(1 - \frac{2z_k}{h}\right) g_{GPL}^{*}, \\ &\text{FG-V:} && g_{GPL}(z_k) = \left(1 + \frac{2z_k}{h}\right) g_{GPL}^{*}, \\ &\text{FG-O:} && g_{GPL}(z_k) = 2\left(1 - \frac{2|z_k|}{h}\right) g_{GPL}^{*}, \\ &\text{FG-X:} && g_{GPL}(z_k) = \frac{4|z_k|}{h} g_{GPL}^{*},\end{aligned} \tag{4}$$

where g^*_{GPL} represents the total mass fraction of the GPLs which is supposed to be same in the bottom and top face sheets. It should be noted that in order to make a fair comparison, in Eq. (4) the

distribution patterns are regulated to have same total mass fraction of the GPLs [14].

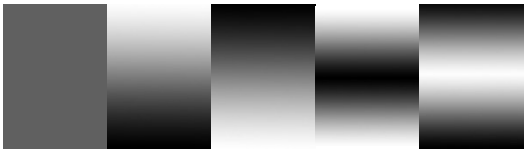

Fig. 2. GPL distribution patterns [14]

Based on the Halpin-Tasai model, the modulus of elasticity (E) can be calculated as follows [15]:

$$E^{(k)}=\left(3\frac{1+\xi_L\eta_L V_{GPL}^{\ b}}{1-\eta_L V_{GPL}^{\ b}}+5\frac{1+\xi_w\eta_w V_{GPL}^{\ b}}{1-\eta_w V_{GPL}^{\ b}}\right)\frac{E_m}{8} \tag{5}$$

in which

$$\eta_L=\frac{\eta-1}{\eta+\xi_L},\ \eta_w=\frac{\eta-1}{\eta+\xi_w},\ \xi_L=2\frac{l_{GPL}}{h_{GPL}}$$
$$\xi_w=2\frac{w_{GPL}}{h_{GPL}},\ \eta=\frac{E_{GPL}}{E_m} \tag{6}$$

2.2 Governing equations

Based on the CPT, the displacement field in the thin face sheets can be considered as

$$\begin{aligned}\hat{u}_k(x,y,z,t)&=u_k(x,y,t)-z_k\frac{\partial w}{\partial x},\\ \hat{v}_k(x,y,z,t)&=v_k(x,y,t)-z_k\frac{\partial w}{\partial y},\\ \hat{w}_k(x,y,z,t)&=w(x,y,t),\end{aligned} \tag{7}$$

where $\hat{u}_k$, $\hat{v}_k$ and $\hat{w}_k$ stand for the displacement in the kth layer in x, y and z directions, respectively, and u_k, v_k and w represent the corresponding displacement at the middle surface of each layer (z_k=0). According to the FSDT, the displacement field in the core (specified with the subscript c) can be stated as follows:

$$\begin{aligned}\hat{u}_2(x,y,z,t)&=u_2(x,y,t)+z_2\alpha_2(x,y,t),\\ \hat{v}_2(x,y,z,t)&=v_2(x,y,t)+z_2\beta_2(x,y,t),\\ \hat{w}_2(x,y,z,t)&=w(x,y,t),\end{aligned} \tag{8}$$

in which α_2 and β_2 show the rotation about y- and x-axes, respectively.

The continuity of displacement between three layers of the plate should be stated as follows:

$$\begin{aligned}\hat{u}_2\left(x,y,-\frac{h_2}{2},t\right)&=\hat{u}_1\left(x,y,\frac{h_1}{2},t\right)\\ \hat{u}_2\left(x,y,\frac{h_2}{2},t\right)&=\hat{u}_3\left(x,y,-\frac{h_3}{2},t\right)\end{aligned} \tag{9}$$

Utilizing Eqs. (7), (8), and (9) and considering same thickness for the face sheets (h_1=h_3=h_f), the following relation can be derived:

$$\begin{aligned}u_2&=\frac{u_1+u_3}{2},\ v_2=\frac{v_1+v_3}{2},\\ \alpha_2&=\frac{u_3-u_1}{h_2}+\frac{h_f}{h_2}\frac{\partial w}{\partial x},\beta_2=\frac{v_3-v_1}{h_2}+\frac{h_f}{h_2}\frac{\partial w}{\partial y}\end{aligned} \tag{10}$$

By substituting Eq. (10) into Eq. (9), the displacement field in the MR core can be stated as follows:

$$\begin{aligned}\hat{u}_2&=\frac{u_1+u_3}{2}+\frac{z_2}{h_2}\left(u_3-u_1+h_f\frac{\partial w}{\partial x}\right)\\ \hat{v}_2&=\frac{v_1+v_3}{2}+\frac{z_2}{h_2}\left(v_3-v_1+h_f\frac{\partial w}{\partial y}\right),\ \hat{w}_2=w\end{aligned} \tag{11}$$

The normal (ε_{ij}) and shear (γ_{ij}) components of the strain tensor in the GPL-reinforced face sheets can be obtained as follows:

$$\begin{aligned}\varepsilon_{xx}^{(k)}&=\frac{\partial\hat{u}_k}{\partial x}=\frac{\partial u_k}{\partial x}-z_k\frac{\partial^2 w}{\partial x^2}\\ \varepsilon_{yy}^{(k)}&=\frac{\partial\hat{v}_k}{\partial y}=\frac{\partial v_k}{\partial y}-z_k\frac{\partial^2 w}{\partial y^2}\\ \gamma_{xy}^{(k)}&=\frac{\partial\hat{u}_k}{\partial y}+\frac{\partial\hat{v}_k}{\partial x}=\frac{\partial u_k}{\partial y}+\frac{\partial v_k}{\partial x}-2z_k\frac{\partial^2 w}{\partial x\,\partial y}\end{aligned} \tag{12}$$

and for the MR core, the following relation can be stated for the shear components of strain:

$$\gamma_{xz}^{(2)}=\frac{\partial \hat{u}_2}{\partial z_2}+\frac{\partial \hat{w}_2}{\partial x}=\frac{u_3-u_1}{h_2}+d\,\frac{\partial w}{\partial x}$$
$$\gamma_{yz}^{(2)}=\frac{\partial \hat{v}_2}{\partial z_2}+\frac{\partial \hat{w}_2}{\partial y}=\frac{v_3-v_1}{h_2}+d\,\frac{\partial w}{\partial y} \quad (13)$$

where

$$d=1+\frac{h_f}{h_2}. \quad (14)$$

The components of the stress tensor in the GPL-reinforced face sheets can be obtained as follows:

$$\begin{Bmatrix}\sigma_{xx}^{(k)}\\ \sigma_{yy}^{(k)}\\ \sigma_{xy}^{(k)}\end{Bmatrix}=\begin{bmatrix}Q_{11}^{(k)} & Q_{12}^{(k)} & 0\\ Q_{12}^{(k)} & Q_{22}^{(k)} & 0\\ 0 & 0 & Q_{66}^{k}\end{bmatrix}\begin{Bmatrix}\varepsilon_{xx}^{(k)}\\ \varepsilon_{yy}^{(k)}\\ \gamma_{xy}^{(k)}\end{Bmatrix}, \quad (15)$$

in which

$$Q_{11}^{(k)}=Q_{22}^{(k)}=\frac{E^{(k)}}{1-\left(\nu^{(k)}\right)^2}$$
$$Q_{12}^{(k)}=\nu^{(k)}Q_{11}^{(k)},\ Q_{66}^{(k)}=\frac{E^{(k)}}{2\left(1+\nu^{(k)}\right)}. \quad (16)$$

It is assumed that the MR core does not bear considerable normal stress; consequently, it can only bear the shear components of the stress tensor which can be stated as

$$\sigma_{xz}^{(2)}=G_2^{*}\gamma_{xz}^{(2)},\quad \sigma_{yz}^{(2)}=G_2^{*}\gamma_{yz}^{(2)}, \quad (17)$$

where G_2^* is known as the complex shear modulus of the MR elastomer.

As stated in Hamilton's principle, by considering t_1 and t_2 as two arbitrary moments and δ as the variational operator, the governing equations and associated boundary conditions can be obtained utilizing the following equations [16]:

$$\int_{t_1}^{t_2}\left(\delta T-\delta U_s+\delta W_{n.c.}\right)dt=0, \quad (18)$$

in which T and U_s respectively indicate the kinetic energy and strain energy, and $W_{n.c.}$ stands for the work done by the external non-conservative loads. The following relation can be considered for the kinetic energy of the plate:

$$T=\sum_{k=1}^{3}\frac{1}{2}\iiint_{V_k}\rho\left[\left(\frac{\partial \hat{u}_k}{\partial t}\right)^2+\left(\frac{\partial \hat{v}_k}{\partial t}\right)^2+\left(\frac{\partial \hat{w}_k}{\partial t}\right)^2\right]dV_k, \quad (19)$$

in which V_k shows the volume of the kth layer:

$$\iiint_{V_k}(\ )\,dV_k=\iint_S\int_{-\frac{h_k}{2}}^{\frac{h_k}{2}}(\ )\,dz_k\,dS. \quad (20)$$

where S shows the surface of the plate. Utilizing the following relation:

$$\int_{-\frac{h_2}{2}}^{\frac{h_2}{2}}\rho z_2\,dz_2=0, \quad (21)$$

Eq. (19) can be stated as follows:

$$T=\frac{1}{2}\iint_S\left\{I_0\left(\frac{\partial w}{\partial t}\right)^2+I_0^{(1)}\left[\left(\frac{\partial u_1}{\partial t}\right)^2+\left(\frac{\partial v_1}{\partial t}\right)^2\right]+I_0^{(3)}\left[\left(\frac{\partial u_3}{\partial t}\right)^2+\left(\frac{\partial v_3}{\partial t}\right)^2\right]-2I_1^{(1)}\left(\frac{\partial u_1}{\partial t}\frac{\partial^2 w}{\partial t\,\partial x}+\frac{\partial v_1}{\partial t}\frac{\partial^2 w}{\partial t\,\partial y}\right)-2I_1^{(3)}\left(\frac{\partial u_3}{\partial t}\frac{\partial^2 w}{\partial t\,\partial x}+\frac{\partial v_3}{\partial t}\frac{\partial^2 w}{\partial t\,\partial y}\right)+\left(I_2^{(1)}+I_2^{(3)}\right)\left[\left(\frac{\partial^2 w}{\partial t\,\partial x}\right)^2+\left(\frac{\partial^2 w}{\partial t\,\partial y}\right)^2\right]+I_0^{(2)}\left[\left(\frac{\partial u_2}{\partial t}\right)^2+\left(\frac{\partial v_2}{\partial t}\right)^2\right]+I_2^{(2)}\left[\left(\frac{\partial \alpha_2}{\partial t}\right)^2+\left(\frac{\partial \beta_2}{\partial t}\right)^2\right]\right\}ds \quad (23)$$

Where

$$I_0^{(k)} = \int_{-\frac{h_k}{2}}^{\frac{h_k}{2}} \rho dz_k,\ I_1^{(k)} = \int_{-\frac{h_k}{2}}^{\frac{h_k}{2}} \rho z_k dz_k$$
$$I_2^{(k)} = \int_{-\frac{h_k}{2}}^{\frac{h_k}{2}} \rho z_k^2 dz_k,\ I_0 = I_0^{(1)} + I_0^{(2)} + I_0^{(3)} \quad (24)$$

The strain energy of plate is stated as follows:

$$U_s = \sum_{k=1}^{3} \frac{1}{2} \iiint_{V_k} \sigma_{ij}^{(k)} \varepsilon_{ij}^{(k)} dV_k, \quad (25)$$

and the variation of the strain energy of plate can be stated as

$$\delta U_s = \sum_{k=1}^{3} \iiint_{V_k} \sigma_{ij}^{(k)} \delta\varepsilon_{ij}^{(k)} dV_k. \quad (26)$$

Eq. (26) can be written in the following expanded form:

$$\delta U_s = \sum_{k=1,3} \iiint_{V_k} \left(\sigma_{xx}^{(k)} \delta\varepsilon_{xx}^{(k)} + \sigma_{yy}^{(k)} \delta\varepsilon_{yy}^{(k)} + \sigma_{xy}^{(k)} \delta\gamma_{xy}^{(k)} \right) dV_k + \iiint_{V_2} \left(\sigma_{xz}^{(2)} \delta\gamma_{xz}^{(2)} + \sigma_{yz}^{(2)} \delta\gamma_{yz}^{(2)} \right) dV_2 \quad (27)$$

which can be written using Eqs. (15), (17), and (20) as follows:

$$\begin{aligned}\delta U_s = \iint_S \Bigg(& N_{xx}^{(1)} \frac{\partial \delta u_1}{\partial x} - M_{xx} \frac{\partial^2 \delta w}{\partial x^2} \\ & + N_{yy}^{(1)} \frac{\partial \delta v_1}{\partial y} - M_{yy} \frac{\partial^2 \delta w}{\partial y^2} + N_{xy}^{(1)} \frac{\partial \delta u_1}{\partial y} \\ & + N_{xy}^{(1)} \frac{\partial \delta v_1}{\partial x} - 2M_{xy} \frac{\partial^2 \delta w}{\partial x \partial y} + N_{xx}^{(3)} \frac{\partial \delta u_3}{\partial x} \\ & + N_{yy}^{(3)} \frac{\partial \delta v_3}{\partial y} + N_{xy}^{(3)} \frac{\partial \delta u_3}{\partial y} + N_{xy}^{(3)} \frac{\partial \delta v_3}{\partial x} \\ & + \frac{Q_{xz}^{(2)}}{h_2} \delta u_3 - \frac{Q_{xz}^{(2)}}{h_2} \delta u_1 + Q_{xz}^{(2)} d \frac{\partial \delta w}{\partial x} \\ & + \frac{Q_{yz}^{(2)}}{h_2} \delta v_3 - \frac{Q_{yz}^{(2)}}{h_2} \delta v_1 + Q_{yz}^{(2)} d \frac{\partial \delta w}{\partial y} \Bigg) dS \end{aligned} \quad (28)$$

where the stress resultants are defined as follows:

$$\begin{Bmatrix} N_{ij}^{(k)} \\ M_{ij}^{(k)} \end{Bmatrix} = \int_{-\frac{h_k}{2}}^{\frac{h_k}{2}} \sigma_{ij}^{(k)} \begin{Bmatrix} 1 \\ z_k \end{Bmatrix} dz_k, \quad ,$$
$$\begin{Bmatrix} Q_{xz}^{(2)} \\ Q_{yz}^{(2)} \end{Bmatrix} = \int_{-\frac{h_2}{2}}^{\frac{h_2}{2}} \begin{Bmatrix} \sigma_{xz}^{(2)} \\ \sigma_{yz}^{(2)} \end{Bmatrix} dz_2 \quad (29)$$
$$M_{xx} = M_{xx}^{(1)} + M_{xx}^{(3)},\ M_{yy} = M_{yy}^{(1)} + M_{yy}^{(3)}$$
$$M_{xy} = M_{xy}^{(1)} + M_{xy}^{(3)}$$

Eq. (29) can be written using Eqs. (12), (13), (15), and (17) as follows:

$$\begin{aligned} N_{xx}^{(k)} &= A_{11}^{(k)} \frac{\partial u_k}{\partial x} + A_{12}^{(k)} \frac{\partial v_k}{\partial y} - B_{11}^{(k)} \frac{\partial^2 w}{\partial x^2} - B_{12}^{(k)} \frac{\partial^2 w}{\partial y^2}, \\ N_{yy}^{(k)} &= A_{12}^{(k)} \frac{\partial u_k}{\partial x} + A_{22}^{(k)} \frac{\partial v_k}{\partial y} - B_{12}^{(k)} \frac{\partial^2 w}{\partial x^2} - B_{22}^{(k)} \frac{\partial^2 w}{\partial y^2}, \\ N_{xy}^{(k)} &= A_{66}^{(k)} \frac{\partial u_k}{\partial y} + A_{66}^{(k)} \frac{\partial v_k}{\partial x} - 2B_{66}^{(k)} \frac{\partial^2 w}{\partial x \partial y}, \\ M_{xx} &= B_{11}^{(1)} \frac{\partial u_1}{\partial x} + B_{11}^{(3)} \frac{\partial u_3}{\partial x} + B_{12}^{(1)} \frac{\partial v_1}{\partial y} \\ &\quad + B_{12}^{(3)} \frac{\partial v_3}{\partial y} - \left(D_{11}^{(1)} + D_{11}^{(3)} \right) \frac{\partial^2 w}{\partial x^2} - \left(D_{12}^{(1)} + D_{12}^{(3)} \right) \frac{\partial^2 w}{\partial y^2}, \\ M_{yy} &= B_{12}^{(1)} \frac{\partial u_1}{\partial x} + B_{12}^{(3)} \frac{\partial u_3}{\partial x} + B_{22}^{(1)} \frac{\partial v_1}{\partial y} + B_{22}^{(3)} \frac{\partial v_3}{\partial y} \\ &\quad - \left(D_{12}^{(1)} + D_{12}^{(3)} \right) \frac{\partial^2 w}{\partial x^2} - \left(D_{22}^{(1)} + D_{22}^{(3)} \right) \frac{\partial^2 w}{\partial y^2}, \\ M_{xy} &= B_{66}^{(1)} \frac{\partial u_1}{\partial y} + B_{66}^{(3)} \frac{\partial u_3}{\partial y} + B_{66}^{(1)} \frac{\partial v_1}{\partial x} \\ &\quad + B_{66}^{(3)} \frac{\partial v_3}{\partial x} - 2 \left(D_{66}^{(1)} + D_{66}^{(3)} \right) \frac{\partial^2 w}{\partial x \partial y} \\ Q_{xz}^{(2)} &= G_2^* \left(u_3 - u_1 + h_2 d \frac{\partial w}{\partial x} \right) \\ Q_{yz}^{(2)} &= G_2^* \left(v_3 - v_1 + h_2 d \frac{\partial w}{\partial y} \right) \end{aligned} \quad (30)$$

in which

$$\begin{Bmatrix} A_{ij}^{(k)} \\ B_{ij}^{(k)} \\ D_{ij}^{(k)} \end{Bmatrix} = \int_{-\frac{h_k}{2}}^{\frac{h_k}{2}} Q_{ij}^{(k)} \begin{Bmatrix} 1 \\ z_k \\ z_k^2 \end{Bmatrix} dz_k. \tag{31}$$

The virtual work done by the external non-conservative loads can be stated as

$$\delta W_{n.c.} = \iint_S q_f \delta w dS, \tag{32}$$

where q_f represents the load per unit area and is stated for the visco-Pasternak foundation as follows:

$$q_f = -k_w w + k_p \left(\frac{\partial^2 w}{\partial x^2} + \frac{\partial^2 w}{\partial y^2} \right) - c \frac{\partial w}{\partial t}, \tag{33}$$

in which k_w, k_p, and c stand for Winkler, Pasternak, and damping coefficients of the foundation.

Substituting Eqs. (23), (28), and (32) into Eq. (18) leads to the following set of the governing equations:

$$\begin{aligned}
&\delta u_1 : \frac{\partial N_{xx}^{(1)}}{\partial x} + \frac{\partial N_{xy}^{(1)}}{\partial y} + \frac{Q_{xz}^{(2)}}{h_2} \\
&-J_0^{(1)} \frac{\partial^2 u_1}{\partial t^2} - J_0^{(2)} \frac{\partial^2 u_3}{\partial t^2} + J_1^{(1)} \frac{\partial^3 w}{\partial t^2 \partial x} = 0, \\
&\delta u_3 : \frac{\partial N_{xx}^{(3)}}{\partial x} + \frac{\partial N_{xy}^{(3)}}{\partial y} - \frac{Q_{xz}^{(2)}}{h_2} - \\
&J_0^{(2)} \frac{\partial^2 u_1}{\partial t^2} - J_0^{(3)} \frac{\partial^2 u_3}{\partial t^2} + J_1^{(3)} \frac{\partial^3 w}{\partial t^2 \partial x} = 0, \\
&\delta v_1 : \frac{\partial N_{yy}^{(1)}}{\partial y} + \frac{\partial N_{xy}^{(1)}}{\partial x} + \frac{Q_{yz}^{(2)}}{h_2} \\
&-J_0^{(1)} \frac{\partial^2 v_1}{\partial t^2} - J_0^{(2)} \frac{\partial^2 v_3}{\partial t^2} + J_1^{(1)} \frac{\partial^3 w}{\partial t^2 \partial y} = 0, \\
&\delta v_3 : \frac{\partial N_{yy}^{(3)}}{\partial y} + \frac{\partial N_{xy}^{(3)}}{\partial x} - \frac{Q_{yz}^{(2)}}{h_2} \\
&-J_0^{(2)} \frac{\partial^2 v_1}{\partial t^2} - J_0^{(3)} \frac{\partial^2 v_3}{\partial t^2} + J_1^{(3)} \frac{\partial^3 w}{\partial t^2 \partial y} = 0,
\end{aligned} \tag{34}$$

$$\begin{aligned}
&\delta w : \frac{\partial^2 M_{xx}}{\partial x^2} + \frac{\partial^2 M_{yy}}{\partial y^2} + 2 \frac{\partial^2 M_{xy}}{\partial x \partial y} \\
&+d \frac{\partial Q_{xz}^{(2)}}{\partial x} + d \frac{\partial Q_{yz}^{(2)}}{\partial y} + q_f - J_1^{(1)} \frac{\partial^3 u_1}{\partial t^2 \partial x} \\
&-J_1^{(3)} \frac{\partial^3 u_3}{\partial t^2 \partial x} - J_1^{(1)} \frac{\partial^2 v_1}{\partial t^2 \partial y} - J_1^{(3)} \frac{\partial^2 v_3}{\partial t^2 \partial y} \\
&+J_2 \frac{\partial^3 w}{\partial t^2 \partial x^2} + J_2 \frac{\partial^3 w}{\partial t^2 \partial y^2} - I_0 \frac{\partial^2 w}{\partial t^2} = 0
\end{aligned}$$

Where

$$\begin{aligned}
&J_0^{(1)} = I_0^{(1)} + \frac{I_0^{(2)}}{4} + \frac{I_2^{(2)}}{h_2^2}, \quad J_1^{(1)} = I_1^{(1)} + \frac{I_2^{(2)} h_f}{h_2^2} \\
&J_0^{(3)} = I_0^{(3)} + \frac{I_0^{(2)}}{4} + \frac{I_2^{(2)}}{h_2^2}, \quad J_0^{(2)} = \frac{I_0^{(2)}}{4} - \frac{I_2^{(2)}}{h_2^2} \\
&J_1^{(3)} = I_1^{(3)} - \frac{I_2^{(2)} h_f}{h_2^2}, \quad J_2 = I_2^{(1)} + I_2^{(3)} + \frac{I_2^{(2)} h_f^2}{h_2^2}
\end{aligned} \tag{35}$$

Substituting Eqs. (30) and (33) into Eq. (34) leads to the following set of the governing equations:

$$\begin{aligned}
&A_{11}^{(1)} \frac{\partial^2 u_1}{\partial x^2} + A_{66}^{(1)} \frac{\partial^2 u_1}{\partial y^2} - \frac{G_2^*}{h_2} u_1 + \frac{G_2^*}{h_2} u_3 \\
&+\left(A_{12}^{(1)} + A_{66}^{(1)} \right) \frac{\partial^2 v_1}{\partial x \partial y} - B_{11}^{(1)} \frac{\partial^3 w}{\partial x^3} \\
&-\left(B_{12}^{(1)} + 2B_{66}^{(1)} \right) \frac{\partial^3 w}{\partial x \partial y^2} + G_2^* d \frac{\partial w}{\partial x} \\
&-J_0^{(1)} \frac{\partial^2 u_1}{\partial t^2} - J_0^{(2)} \frac{\partial^2 u_3}{\partial t^2} + J_1^{(1)} \frac{\partial^3 w}{\partial t^2 \partial x} = 0, \\
&\frac{G_2^*}{h_2} u_1 + A_{11}^{(3)} \frac{\partial^2 u_3}{\partial x^2} + A_{66}^{(3)} \frac{\partial^2 u_3}{\partial y^2} - \frac{G_2^*}{h_2} u_3 \\
&+\left(A_{12}^{(3)} + A_{66}^{(3)} \right) \frac{\partial^2 v_3}{\partial x \partial y} - B_{11}^{(3)} \frac{\partial^3 w}{\partial x^3} \\
&-\left(B_{12}^{(3)} + 2B_{66}^{(3)} \right) \frac{\partial^3 w}{\partial x \partial y^2} - G_2^* d \frac{\partial w}{\partial x} \\
&-J_0^{(2)} \frac{\partial^2 u_1}{\partial t^2} - J_0^{(3)} \frac{\partial^2 u_3}{\partial t^2} + J_1^{(3)} \frac{\partial^3 w}{\partial t^2 \partial x} = 0,
\end{aligned}$$

$$\left(A_{12}^{(1)}+A_{66}^{(1)}\right)\frac{\partial^2 u_1}{\partial x\,\partial y}+A_{66}^{(1)}\frac{\partial^2 v_1}{\partial x^2}+A_{22}^{(1)}\frac{\partial^2 v_1}{\partial y^2}$$
$$-\frac{G_2^*}{h_2}v_1+\frac{G_2^*}{h_2}v_3-\left(B_{12}^{(1)}+2B_{66}^{(1)}\right)\frac{\partial^3 w}{\partial x^2\partial y}$$
$$-B_{22}^{(1)}\frac{\partial^3 w}{\partial y^3}+G_2^* d\frac{\partial w}{\partial y}-J_0^{(1)}\frac{\partial^2 v_1}{\partial t^2}$$
$$-J_0^{(2)}\frac{\partial^2 v_3}{\partial t^2}+J_1^{(1)}\frac{\partial^3 w}{\partial t^2\partial y}=0,$$

$$\left(A_{12}^{(3)}+A_{66}^{(3)}\right)\frac{\partial^2 u_3}{\partial x\,\partial y}+\frac{G_2^*}{h_2}v_1+A_{66}^{(3)}\frac{\partial^2 v_3}{\partial x^2}$$
$$+A_{22}^{(3)}\frac{\partial^2 v_3}{\partial y^2}-\frac{G_2^*}{h_2}v_3-\left(B_{12}^{(3)}+2B_{66}^{(3)}\right)\frac{\partial^3 w}{\partial x^2\partial y}$$
$$-B_{22}^{(3)}\frac{\partial^3 w}{\partial y^3}-G_2^* d\frac{\partial w}{\partial y}-J_0^{(2)}\frac{\partial^2 v_1}{\partial t^2}$$
$$-J_0^{(3)}\frac{\partial^2 v_3}{\partial t^2}+J_1^{(3)}\frac{\partial^3 w}{\partial t^2\partial y}=0,$$

$$B_{11}^{(1)}\frac{\partial^3 u_1}{\partial x^3}+\left(B_{12}^{(1)}+2B_{66}^{(1)}\right)\frac{\partial^3 u_1}{\partial x\,\partial y^2}-G_2^* d\frac{\partial u_1}{\partial x}$$
$$+B_{11}^{(3)}\frac{\partial^3 u_3}{\partial x^3}+\left(B_{12}^{(3)}+2B_{66}^{(3)}\right)\frac{\partial^3 u_3}{\partial x\,\partial y^2}+G_2^* d\frac{\partial u_3}{\partial x}$$
$$+\left(B_{12}^{(1)}+2B_{66}^{(1)}\right)\frac{\partial^3 v_1}{\partial x^2\partial y}+B_{22}^{(1)}\frac{\partial^3 v_1}{\partial y^3}-G_2^* d\frac{\partial v_1}{\partial y}$$
$$+\left(B_{12}^{(3)}+2B_{66}^{(3)}\right)\frac{\partial^3 v_3}{\partial x^2\partial y}+B_{22}^{(3)}\frac{\partial^3 v_3}{\partial y^3}+G_2^* d\frac{\partial v_3}{\partial y}$$
$$-\left(D_{11}^{(1)}+D_{11}^{(3)}\right)\frac{\partial^4 w}{\partial x^4}$$
$$-2\left[D_{12}^{(1)}+D_{12}^{(3)}+2\left(D_{66}^{(1)}+D_{66}^{(3)}\right)\right]\frac{\partial^4 w}{\partial x^2\partial y^2}$$
$$+\left(G_2^* h_2 d^2+k_p\right)\frac{\partial^2 w}{\partial x^2}$$
$$-\left(D_{22}^{(1)}+D_{22}^{(3)}\right)\frac{\partial^4 w}{\partial y^4}+\left(G_2^* h_2 d^2+k_p\right)\frac{\partial^2 w}{\partial y^2}$$
$$-k_w w-c\frac{\partial w}{\partial t}-J_1^{(1)}\frac{\partial^3 u_1}{\partial t^2\partial x}-J_1^{(3)}\frac{\partial^3 u_3}{\partial t^2\partial x}$$
$$-J_1^{(1)}\frac{\partial^2 v_1}{\partial t^2\partial y}-J_1^{(3)}\frac{\partial^2 v_3}{\partial t^2\partial y}+J_2\frac{\partial^3 w}{\partial t^2\partial x^2}$$
$$+J_2\frac{\partial^3 w}{\partial t^2\partial y^2}-I_0\frac{\partial^2 w}{\partial t^2}=0. \qquad (36)$$

3. Solution procedure

Using Navier's method, the following solution can be considered for a simply supported plate:

$$u_k(x,y,t)=\sum_{m=1}^{\infty}\sum_{n=1}^{\infty}U_{mn}^{(k)}e^{i\omega t}\cos(\alpha x)\sin(\beta y)$$
$$v_k(x,y,t)=\sum_{m=1}^{\infty}\sum_{n=1}^{\infty}V_{mn}^{(k)}e^{i\omega t}\sin(\alpha x)\cos(\beta y) \qquad (37)$$
$$w(x,y,t)=\sum_{m=1}^{\infty}\sum_{n=1}^{\infty}W_{mn}e^{i\omega t}\sin(\alpha x)\sin(\beta y)$$

where $i^2=-1$, and

$$\alpha=\frac{m\pi}{a},\quad \beta=\frac{n\pi}{b}. \qquad (38)$$

Substituting Eq. (37) into Eq. (36) leads to the following algebraic equation:

$$\left(\omega^2[M]+\omega[C]+[K]\right)\{s\}=\{0\} \qquad (39)$$

in which

$$\{s\}=\begin{Bmatrix} U_{mn}^{(1)} \\ U_{mn}^{(3)} \\ V_{mn}^{(1)} \\ V_{mn}^{(3)} \\ W_{mn} \end{Bmatrix}$$

$$[M]=\begin{bmatrix} J_0^{(1)} & J_0^{(2)} & 0 & 0 & -\alpha J_1^{(1)} \\ J_0^{(2)} & J_0^{(3)} & 0 & 0 & -\alpha J_1^{(3)} \\ 0 & 0 & J_0^{(1)} & J_0^{(2)} & -\beta J_1^{(1)} \\ 0 & 0 & J_0^{(2)} & J_0^{(3)} & -\beta J_1^{(3)} \\ -\alpha J_1^{(1)} & -\alpha J_1^{(3)} & -\beta J_1^{(1)} & -\beta J_1^{(3)} & \left(\alpha^2+\beta^2\right)J_2 \\ & & & & +I_0 \end{bmatrix} \quad (40)$$

$$[C]=-ic\begin{bmatrix} 0&0&0&0&0 \\ 0&0&0&0&0 \\ 0&0&0&0&0 \\ 0&0&0&0&0 \\ 0&0&0&0&1 \end{bmatrix}$$

$$[K]=\begin{bmatrix} K_{11} & K_{12} & K_{13} & 0 & K_{15} \\ K_{21} & K_{22} & 0 & K_{24} & K_{25} \\ K_{31} & 0 & K_{33} & K_{34} & K_{35} \\ 0 & K_{42} & K_{43} & K_{44} & K_{45} \\ K_{51} & K_{52} & K_{53} & K_{54} & K_{55} \end{bmatrix}$$

$$K_{11}=-\left(\alpha^2 A_{11}^{(1)}+\beta^2 A_{66}^{(1)}+\frac{G_2^*}{h_2}\right),\quad K_{12}=\frac{G_2^*}{h_2},$$

$$K_{13}=-\alpha\beta\left(A_{12}^{(1)}+A_{66}^{(1)}\right)$$

$$K_{15}=\alpha^3 B_{11}^{(1)}+\alpha\beta^2\left(B_{12}^{(1)}+2B_{66}^{(1)}\right)+\alpha d G_2^*,$$

$$K_{22}=-\left(\alpha^2 A_{11}^{(3)}+\beta^2 A_{66}^{(3)}+\frac{G_2^*}{h_2}\right)$$

$$K_{24}=-\alpha\beta\left(A_{12}^{(3)}+A_{66}^{(3)}\right),$$

$$K_{25}=\alpha^3 B_{11}^{(3)}+\alpha\beta^2\left(B_{12}^{(3)}+2B_{66}^{(3)}\right)-\alpha d G_2^*$$

$$K_{33}=-\left(\alpha^2 A_{66}^{(1)}+\beta^2 A_{22}^{(1)}+\frac{G_2^*}{h_2}\right),\quad K_{34}=\frac{G_2^*}{h_2},$$

$$K_{35}=\alpha^2\beta\left(B_{12}^{(1)}+2B_{66}^{(1)}\right)+\beta^3 B_{22}^{(1)}+\beta d G_2^*,$$

$$K_{44}=-\left(\alpha^2 A_{66}^{(3)}+\beta^2 A_{22}^{(3)}+\frac{G_2^*}{h_2}\right)$$

$$K_{45}=\alpha^2\beta\left(B_{12}^{(3)}+2B_{66}^{(3)}\right)+\beta^3 B_{22}^{(3)}-\beta d G_2^*,$$

$$K_{55}=-\left\{\alpha^4\left(D_{11}^{(1)}+D_{11}^{(3)}\right)\right.$$

$$\left.+2\alpha^2\beta^2\left[D_{12}^{(1)}+D_{12}^{(3)}+2\left(D_{66}^{(1)}+D_{66}^{(3)}\right)\right]\right.$$

,

4. Numerical results

In this section, numerical examples are provided for the presented model. Except for the cases which are mentioned directly, a sandwich rectangular plate of a=1 m, b/a=2, h_2/a=0.02, and h_f/a=0.01 is considered. The face sheets are made of epoxy as the matrix (E_m=3 GPa, ν_m=0.3, and ρ_m=1200 kg/m^3 [17]) reinforced with GPLs (E_{GPL}=1.01 TPa, ν_{GPL}=0.186, ρ_{GPL}=1060 kg/m^3 [17]) of dimensions l_{GPL}/a=10^{-6}, w_{GPL}/l_{GPL}=0.5, h_{GPL}/l_{GPL}=0.001. The GPLs are distributed based on the FG-A pattern at the bottom layer and FG-V pattern at the top layer (denoted by A-V) with total mass fraction g^*_{GPL}=0.01. An MRE is selected as the core consisted of 10 % natural rubber, 80 % iron particles, and 10 % plasticizer. The complex shear modulus of this MRE is reported experimentally in term of the magnetic field intensity ($0\le B\le 1$ T) as follows [3, 18]:

$$\begin{aligned} &G_2^*=G_0\left(1+\eta_0 j\right),\\ &G_0=-6.9395B^6-9.1077B^5+71.797B^4\\ &-93.422B^3+38.778B^2+2.43B+2.7006\quad MPa,\\ &\eta_0=5.3485B^6-17.787B^5+22.148B^4\\ &-12.185B^3+2.3522B^2+0.1526B+0.228, \end{aligned} \quad (41)$$

where G_0 and η_0 are known as the shear storage modulus and loss factor of the MR material. The density of the MRE is considered as ρ_2=3500 kg/m^3 [5] and the magnetic field intensity is selected as B=0.5 T. The dimensionless form of the natural frequencies and coefficients of the foundation are defined as follows:

$$\begin{aligned} &\lambda_{mn}=\Omega_{mn}a\sqrt{\frac{\rho_m}{E_m}},\ k_w^*=\frac{k_w a}{E_m}\\ &k_p^*=\frac{k_p}{E_m a},\ c^*=\frac{c}{\sqrt{\rho_m E_m}} \end{aligned} \quad (42)$$

in which k^*_w=0.01, k^*_p=0.0001 and c^*=0.01 are selected.

To validate the presented analysis, consider a rectangular sandwich plate with a viscoelastic core and isotropic homogenous face sheets. Dimensions of the plate are considered as a=0.3048 m, b=0.3480 m, h_2=0.254 mm, and h_f=0.762 mm; the mechanical properties of the face sheets are selected as E_f=68.9 GPa, ν_f=0.3, and ρ_f=2740 kg/m^3; and the complex shear modulus and density of the core are considered as G^*_2=0.896(1+0.5j) MPa and ρ_2=999 kg/m^3, respectively. For various vibrational modes, values of the natural frequencies and corresponding loss factors are presented in Table 1 against those reported by Refs. [19, 20]. As observed, results are in high agreement which confirms the accuracy of the presented analysis.

Table 1. Validation of the present study

(m,n)	Present		Johnson and Kienholz [19]		Cupiał and Nizioł [20]	
	Ω_{mn} (Hz)	η_{mn}	Ω_{mn} (Hz)	η_{mn}	Ω_{mn} (Hz)	η_{mn}
(1,1)	60.24	0.190	60.30	0.190	60.20	0.190
(1,2)	115.3	0.203	115.4	0.203	115.2	0.203
(2,1)	130.5	0.199	130.6	0.199	130.2	0.199
(2,2)	178.5	0.181	178.7	0.181	178.5	0.181
(1,3)	195.5	0.174	195.7	0.174	195.4	0.174

Fig. 3 shows the influences of magnetic field intensity on the natural frequencies and loss factors of the plate. As shown in this figure, by increasing the magnetic field intensity from B=0 to almost B=0.6 T, natural frequencies increase which can be explained by the growth in the value of the shear storage modulus and consequently increases in the stiffness of the plate. As observed, by increasing the magnetic field intensity to higher values (B>0.6 T) no significant increase in the natural frequencies can be seen which confirms the saturation of the MRE core at B≈0.6 T. Fig. 3 shows that there is an optimum value for the magnetic field intensity which creates the maximum values of the loss factor in all vibrational modes. At this optimum value of the magnetic field intensity, the maximum damping can be achieved.

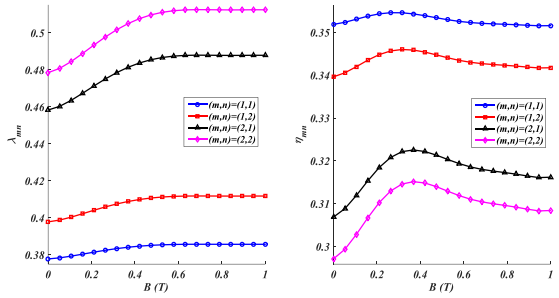

Fig. 3. Effects of magnetic field intensity on the natural frequencies and loss factor

Fig. 4 is devoted to studying the effects of the aspect ratio (length) of the plate on the natural frequencies and loss factors of the plate. As this figure shows, by increasing the aspect ratio of the plate, natural frequency decreases, and loss factor increases in all vibrational modes. An increase in the length of the plate leads to a decrease in the stiffness and an increase in the mass of the plate which reduces the natural frequencies of the plate. Fig. 4 confirms that for higher values of the aspect ratio, natural frequencies and corresponding loss factors tend to specific values, independently from the wave number n. These values are corresponding natural frequencies and loss factors of an infinitely long plate in the y-axis direction (a simply supported strip).

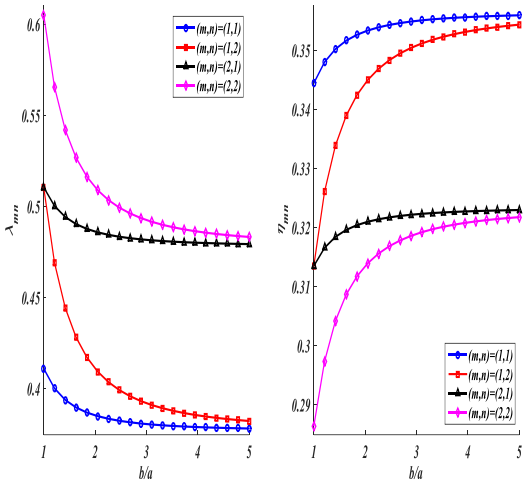

Fig. 4. Effects of aspect ratio of the plate on the natural frequencies and loss factor

The effects of the thickness of the MR core on the natural frequencies and loss factors of the plate are studied in Fig. 5. As the MR core has a high density and low stiffness, an increase in the thickness of the MR core leads to a considerable increase in the mass of the plate and a small increase in the stiffness of the plate; consequently, by increasing the thickness of the MR core the natural frequency decreases in all vibrational modes. Fig. 5 also shows that by increasing the thickness of the MR core the loss factor decreases in all vibrational modes which reveals that a thinner MR core has a higher capacity to damp the vibration of the plate.

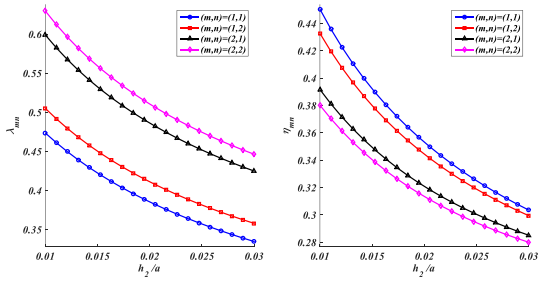

Fig. 5. Effects of thickness of the MR core on the natural frequencies and loss factor

Fig. 6 shows the influences of the thickness of GPL-reinforced face sheets on the natural frequencies and loss factors of the plate. An increase in the thickness of GPL-reinforced face sheets leads to growth in both stiffness and mass of the plate and as shown in Fig. 6, no specific trend can be found for the variation of the natural frequencies versus variation of the thickness of GPL-reinforced face. This figure also shows that by increasing the thickness of GPL-reinforced face sheets the loss factor diminishes in all vibrational modes.

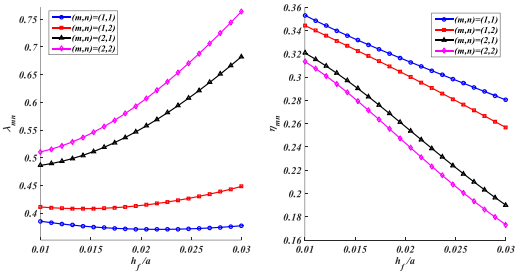

Fig. 6. Effects of the thickness of GPL-reinficed face sheets on the natural frequencies and loss factor

Fig. 7 shows the effects of the total mass fraction of the GPLs on natural frequencies and loss factors of the plate. As observed, subjoining a small amount of GPLs to the matrix leads to remarkable growth

in the natural frequencies. It can be explained by the high value of the modulus of elasticity of the GPLs which is significantly greater than the modulus of elasticity of the epoxy. Fig. 7 also shows that no specific trend can be reported for the variation of the loss factor versus variation of the total mass fraction of the GPLs.

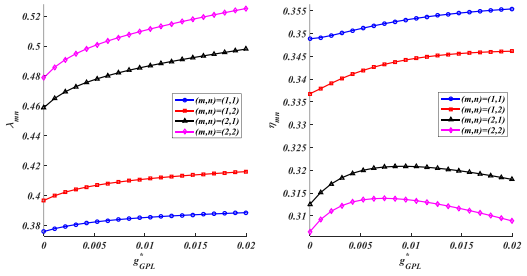

Fig. 7. Effects of total mass fraction of the GPLs on the natural frequencies and loss factor

Table 2 presents values of natural frequencies of the plate for some selected GPL distribution patterns at the bottom and top layers. This table reveals that depending on the mode number, the highest values of natural frequencies belong to X-X and A-V pattern, the lowest ones belong to O-O pattern. In other words, in order to make the most increase in the values of natural frequencies, it is better to distribute the GPL as far as away from the middle surfaces of the bottom and top face sheets. This table reveals that no specific trend can be detected for the effect of GPL distributions pattern on the loss factor. It is noteworthy that the results provided in Table 2 can be utilized as benchmark data for other authors to validate their works.

Table 2. Effects of distribution pattern of the GPLs on the natural frequencies and loss factor

	λ_{mn}				η_{mn}			
	(1,1)	(1,2)	(2,1)	(2,2)	(1,1)	(1,2)	(2,1)	(2,2)
U-U	0.3833	0.4080	0.4817	0.5060	0.3525	0.3427	0.3159	0.3076
A-A	0.3830	0.4072	0.4785	0.5018	0.3529	0.3435	0.3184	0.3107
O-O	0.3826	0.4063	0.4752	0.4975	0.3532	0.3443	0.3210	0.3139
X-X	0.3840	0.4097	0.4881	0.5145	0.3518	0.3412	0.3111	0.3016
A-V	0.3853	0.4110	0.4862	0.5105	0.3532	0.3444	0.3208	0.3135
O-X	0.3826	0.4063	0.4752	0.4975	0.3532	0.3443	0.3210	0.3139
U-V	0.3843	0.4095	0.4839	0.5082	0.3529	0.3435	0.3184	0.3105

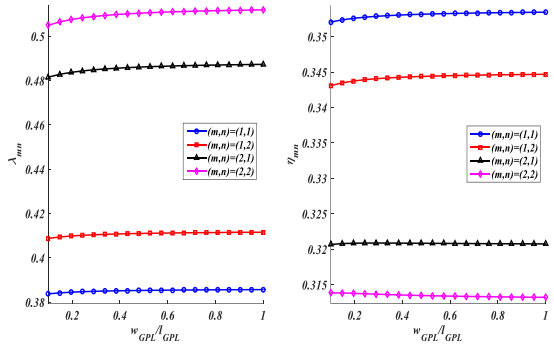

Fig. 8. Effects of aspect ratio of the GPLs on the natural frequencies and loss factor

Variation of natural frequencies of the plate versus variation of the width of GPLs is illustrated in Fig. 8. As observed, an increase in the width of GPLs slightly increases the natural frequencies of the plate. To explain this it should be noticed that an increase in the width of the GPLs increases the specific surface area of them which provides a stronger bonding with the matrix. Fig. 8 also shows that no specific trend can be detected for the variation of the loss factor versus variation of the width of the GPLs.

Fig. 9 is provided to examine the influence of the thickness of the GPLs on the natural frequencies and loss factors of the plate. As observed, by increasing the thickness of the GPLs a slight reduction can be seen in the natural frequencies. This figure also shows no specific trend for the variation of the loss factor versus variation of the thickness of the GPLs. Figs. 8 and 9 demonstrate that in order to have a better reinforcing effect, GPLs with larger surface area and fewer monolayer graphene sheets should be utilized.

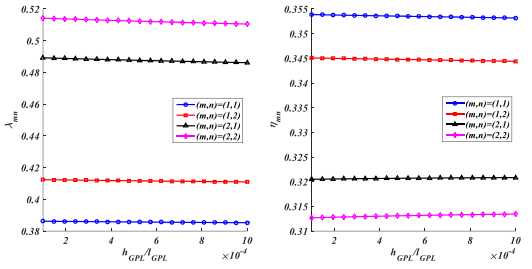

Fig. 9. Effects of thickness of the GPLs on the natural frequencies and loss factor

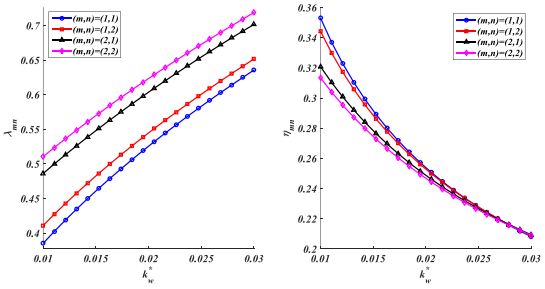

Fig. 10. Effects of Winkler coefficient of the foundation on the natural frequencies and loss factor

Figs. 10 and 11 are depicted to examine the influences of the Winkler and Pasternak coefficients of the foundation on the natural frequencies of the plate and corresponding loss factors. As observed, by increasing the Winkler and Pasternak coefficients of the foundation natural frequency grows in all vibrational modes which can be explained by an increase in the stiffness of the plate-foundation system. These figures also show that an increase in the Winkler and Pasternak coefficients of the foundation reduces the loss factors of the plate. In other words, a stiffer foundation decreases the rate of damping in all vibrational modes.

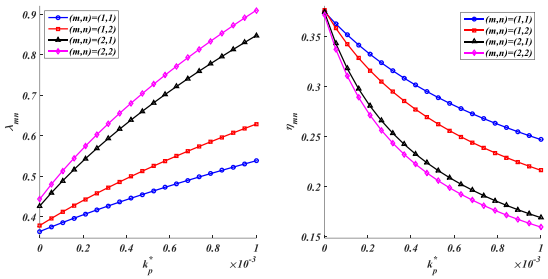

Fig. 11. Effects of Pasternak coefficient of the foundation on the natural frequencies and loss factor

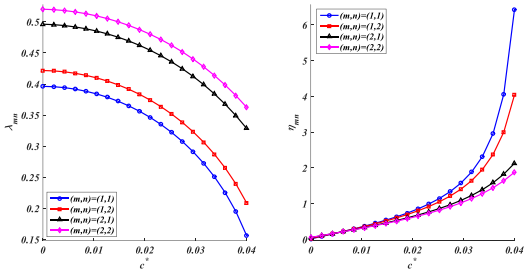

Fig. 12. Effects of damping coefficient of the foundation on the natural frequencies and loss factor

The influences of the damping coefficient of the foundation on the natural frequencies of the plate and corresponding loss factors are investigated in Fig. 12. As observed, by increasing the damping coefficient of the foundation natural frequency decreases, and loss factor increases in all vibrational modes which can be explained by an increase in energy dissipation of the foundation. It should be noted that by increasing the damping coefficient of the foundation the natural frequency of each vibrational mode tend to zero and critical and supercritical behavior can be defined for these vibrational modes.

5. Conclusion

In this paper, an analytical solution was provided for free vibrational characteristics of three-layered sandwich plates with magneto-rheological (MR) core and GPL-reinforced face sheets resting on a visco-Pasternak foundation. The most findings of this paper can be stated as follows:

- By increasing the magnetic field intensity from zero to a specific value, the natural frequencies grow; but, by increasing the magnetic field intensity to higher values no remarkable increase in the natural frequencies can be detected.
- There is an optimum value for the magnetic field intensity which leads to the maximum values of the loss factor in all vibrational modes.
- By increasing the length of the plate, natural frequency decreases, and loss factor increases in all vibrational modes.
- By increasing the thickness of the MR core the natural frequency and loss factor decrease in all vibrational modes.
- By increasing the thickness of GPL-reinforced face sheets the loss factor decreases in all vibrational modes; but, no specific trend can be found for the variation of the natural frequencies versus variation of the thickness of GPL-reinforced face.
- Subjoining a small amount of GPLs to the matrix leads to a significant increase in the natural frequencies.
- In order to have a better reinforcing effect, GPLs with larger surface area and fewer monolayer graphene sheets should be utilized and it is more helpful to distribute them as far as away from the middle surfaces of the bottom and top face sheets.

- By increasing the Winkler and Pasternak coefficients of the foundation natural frequency increases and loss factor decreases in all vibrational modes.
- By increasing the damping coefficient of the foundation natural frequency decreases, and loss factor increases in all vibrational modes.
- No specific trends can be reported for the variation of the loss factors versus variation of the total mass fraction, distributions pattern, surface area, and thickness of the GPLs.

Reference

[1] Lara-Prieto V, Parkin R, Jackson M, Silberschmidt V, Kęsy Z. Vibration characteristics of MR cantilever sandwich beams: experimental study. Smart Materials and structures. 2009;19:015005.

[2] Nayak B, Dwivedy S, Murthy K. Dynamic analysis of magnetorheological elastomer-based sandwich beam with conductive skins under various boundary conditions. Journal of Sound and Vibration. 2011;330:1837-59.

[3] Nayak B, Dwivedy S, Murthy K. Dynamic stability of a rotating sandwich beam with magnetorheological elastomer core. European Journal of Mechanics-A/Solids. 2014;47:143-55.

[4] Rajamohan V, Sundararaman V, Govindarajan B. Finite element vibration analysis of a magnetorheological fluid sandwich beam. Procedia Engineering. 2013;64:603-12.

[5] Navazi H, Bornassi S, Haddadpour H. Vibration analysis of a rotating magnetorheological tapered sandwich beam. International Journal of Mechanical Sciences. 2017;122:308-17.

[6] Rokn-Abadi MR, Shahali P, Haddadpour H. Effects of magnetoelastic loads on free vibration characteristics of the magnetorheological-based sandwich beam. Journal of Intelligent Material Systems and Structures. 2020;31:1015-28.

[7] Omidi Soroor A, Asgari M, Haddadpour H. Effect of axially graded constraining layer on the free vibration properties of three layered sandwich beams with magnetorheological fluid core. Composite Structures. 2021;255:112899.

[8] Aguib S, Nour A, Zahloul H, Bossis G, Chevalier Y, Lançon P. Dynamic behavior analysis of a magnetorheological elastomer sandwich plate. International Journal of Mechanical Sciences. 2014;87:118-36.

[9] Payganeh G, Malekzadeh K, Malek Mohammadi H. Free vibration of sandwich panels with smart magneto-rheological layers and flexible cores. Journal of Solid Mechanics. 2016;8:12-30.

[10] Yeh J-Y. Vibration characteristics analysis of orthotropic rectangular sandwich plate with magnetorheological elastomer. Procedia Engineering. 2014;79:378-85.

[11] Eshaghi M. The effect of magnetorheological fluid and aerodynamic damping on the flutter boundaries of MR fluid sandwich plates in supersonic airflow. European Journal of Mechanics-A/Solids. 2020;82:103997.

[12] Afshari H. Free vibration analysis of GNP-reinforced truncated conical shells with different boundary conditions. Australian Journal of Mechanical Engineering. 2020:1-17.

[13] Afshari H. Effect of graphene nanoplatelet reinforcements on the dynamics of rotating truncated conical shells. Journal of the Brazilian Society of Mechanical Sciences and Engineering. 2020;42:1-22.

[14] Afshari H, Adab N. Size-dependent buckling and vibration analyses of GNP reinforced microplates based on the quasi-3D sinusoidal shear deformation theory. Mechanics Based Design of Structures and Machines. 2020:1-22.

[15] Affdl JH, Kardos J. The Halpin-Tsai equations: a review. Polymer Engineering & Science. 1976;16:344-52.

[16] Reddy JN. Energy principles and variational methods in applied mechanics. Hoboken, New Jersey: John Wiley & Sons, 2017.

[17] Jeawon Y, Drosopoulos G, Foutsitzi G, Stavroulakis G, Adali S. Optimization and analysis of frequencies of multi-scale graphene/fibre reinforced nanocomposite laminates with non-uniform distributions of reinforcements. Engineering Structures. 2021;228:111525.

[18] Chen L, Gong X-l, Jiang W-q, Yao J-j, Deng H-x, Li W-h. Investigation on magnetorheological elastomers based on natural rubber. Journal of Materials Science. 2007;42:5483-9.

[19] Johnson CD, Kienholz DA. Finite element prediction of damping in structures with constrained viscoelastic layers. AIAA journal. 1982;20:1284-90.

[20] Cupiał P, Niziół J. Vibration and damping analysis of a three-layered composite plate with a viscoelastic mid-layer. Journal of Sound and Vibration. 1995;183:99-114.